Distributed Coordination of Multi-microgrids in Active Distribution Networks for Provisioning Ancillary Services

Mallick, Arghya; Mishra, Abhishek; Hota, Ashish R.; Bajpai, Prabodh

DOI
10.1109/JSYST.2024.3404600

Publication date
2024

Document Version
Final published version

Published in
IEEE Systems Journal

Distributed Coordination of Multi-microgrids in Active Distribution Networks for Provisioning Ancillary Services

Arghya Mallick, *Student Member, IEEE*, Abhishek Mishra, *Student Member, IEEE*, Ashish R. Hota, *Senior Member, IEEE*, and Prabodh Bajpai, *Senior Member, IEEE*

***Abstract*—With the phenomenal growth in renewable energy generation, the conventional synchronous generator-based power plants are gradually getting replaced by renewable energy sources-based microgrids. Such transition gives rise to the challenges of procuring various ancillary services from microgrids. We propose a distributed optimization framework that coordinates multiple microgrids in an active distribution network for provisioning passive voltage support-based ancillary services while satisfying operational constraints. Specifically, we exploit the reactive power support capability of the inverters and the flexibility offered by storage systems available with microgrids for provisioning ancillary service support to the transmission grid. We develop novel mixed-integer inequalities to represent the set of feasible active and reactive power exchange with the transmission grid that ensures passive voltage support. The proposed alternating direction method of multipliers-based algorithm is fully distributed, and does not require the presence of a centralized entity to achieve coordination among the microgrids. We present detailed numerical results on the IEEE 33-bus distribution test system to demonstrate the effectiveness of the proposed approach and examine the scalability and convergence behavior of the distributed algorithm for different choice of hyperparameters and network sizes.**

***Index Terms*—Active distribution network (ADN), alternating direction method of multipliers (ADMM), ancillary services, distributed optimization, microgrids.**

NOMENCLATURE

A. Sets

$[M]$	Set of integers defined as $\{1, 2, \ldots, M\}$.
$\mathbb{R}$	Set of real numbers.
$\mathcal{C}_i$	Children nodes of the node i.
$\mathcal{E}$	Communication links between agents.
$\mathcal{M}$	Bus indices in a distribution network (DN) where microgrids are located.
$\mathcal{N}_i$	Neighbor nodes for agent i.
$\mathcal{T}$	Nodes of a DN.
$\mathcal{U}$	Indices of lines of a DN.
$\mathcal{V}$	Indices for agents in the distributed framework.

B. Parameters

β^b	Penalty for battery storage usage.
β^c	Penalty for load curtailment.
β^{loss}	Penalty for energy loss in distribution lines.
β^p	Tariff (€/kWh) for energy exchange between TN and DN.
η	Product of average efficiency of battery and sampling time of the optimization problem.
Ω	Power factor angle of load at microgrid.
ϕ	Power factor angle in the passive voltage support curve.
ρ	Penalty factor for the regularizer term in subproblems of agents.
c^p	Penalty factor (in € /KVAR) for passive voltage support scheme.
$E_{\text{min/max}}$	Min./max. energy level of battery storage.
M^p	"Big-M" constant used for integer constraints.
N_b	Number of buses of a network.
N_l	Number of lines of a DN.
N_m	Number of microgrids.
N_p	Prediction horizon.
$P^{\text{bat}}_{\text{min/max}}$	Min./max. power discharge/charge level of battery storage.
$P^{\text{load,ac}}$	AC load of microgrid.
P^{load}	Total active power load at the microgrids.
P^{pv}	PV generation power at microgrids.
Q^{load}	Total reactive power loads at the microgrids.
r_j	Resistance of distribution line j.
S^{inv}	Maximum apparent power rating of an inverter.
S_j^{max}	Maximum apparent power handling capability of distribution line j.
S_{tr}	Nominal apparent power of the transformer.
$V^{\text{max/min}}$	Max/min voltage magnitude limits of buses.
V_{tr}	Short-circuit voltage of substation transformer.
x_j	Inductance of distribution line j.

Manuscript received 8 January 2024; revised 12 April 2024; accepted 16 May 2024. Date of publication 17 June 2024; date of current version 20 September 2024. This work was supported in part by the Science and Engineering Research Board (SERB), Government of India, through IMPRINT-IIC scheme under Grant IMP/2019/000451/EN and in part by SERB sponsored Center of Excellence on Energy Aware Urban Infrastructure, IIT Kharagpur, under Grant IPA/2021/000081. The work of Abhishek Mishra was supported by the Prime Minister's Research Fellowship. *(Corresponding author: Arghya Mallick.)*

Arghya Mallick is with the Delft Centre for Systems and Control, Delft University of Technology, 2628 Delft, The Netherlands (e-mail: a.mallick@tudelft.nl).

Abhishek Mishra and Ashish R. Hota are with the Department of Electrical Engineering, Indian Institute of Technology Kharagpur, Kharagpur 721302, India (e-mail: abhishekmishra.ee21@kgpian.iitkgp.ac.in; ahota@ee.iitkgp.ac.in).

Prabodh Bajpai is with the Department of Sustainable Energy Engineering, Indian Institute of Technology Kanpur, Kanpur 208016, India (e-mail: pbajpai@iitk.ac.in).

Digital Object Identifier 10.1109/JSYST.2024.3404600

C. Variables

λ_i	Lagarangian multiplier of agent i.
C^{tn}	Penalty for violation of passive voltage support scheme.
E	Energy available with the storage elements.
I^{sq}	Square of the line current magnitude.
P, Q	Active and reactive power flow on distribution lines.
P^{bat}	Charging/discharging power of battery storage.
P^{curt}	Curtailment of loads.
$P^{\text{ex}}, Q^{\text{ex}}$	Active and reactive power exchange with transmission network.
$P^{\text{inj}}, Q^{\text{inj}}$	Active and reactive power injections at the nodes of a network.
P^{inv}	Active power flowing through the inverter of microgrid.
Q^{inv}	Reactive power generation/absorption by the inverters at microgrids.
V^{sq}	Square of bus voltage magnitude.

I. Introduction

ANCILLARY services (ASs), such as frequency control, voltage control, and ramping support, play an essential role in reliable and resilient power systems operation [1], [2], [3], [4], [5]. Due to major shift toward renewable energy sources (RESs) integrated power system, the synchronous generator-based power plants are gradually phasing out resulting in diminished source of reactive power in the transmission network, which is poised to disturb voltage regulation of the system in long run [6]. In view of voltage control-based AS, transmission system operators (TSOs) have invested considerable capital in voltage regulating devices, such as capacitor banks, static vol-ampere-reactive (VAR) compensators, and tap changing transformers. Although these devices perform effectively, they incur high capital cost, which is uneconomical [7]. Consequently, TSOs are increasingly seeking to tap into flexibility resources available at active distribution networks (ADNs) that include distributed energy resources (DERs), storage units, microgrids, and smart buildings for procuring AS. However, extracting such flexibility from ADNs is quite challenging as it requires suitable coordination and optimization of these multitude of entities subject to stringent operational constraints.

In connection with this, authors in [8] proposed a centralized optimal power flow problem to optimize DN operation and also provide voltage support to the transmission network considering operational constraints of the ADN and microgrids (MGs). Similarly, a recent work [9] leveraged the flexibility offered by smart buildings (with its local generation and storage units) present in the low-voltage network to provide voltage support to the medium-voltage network. The authors considered a hierarchical optimization approach where smart buildings solve their local energy management problems while responding to suitable signals sent by the ADN. Provisioning voltage ancillary services to the transmission system by utilizing static compensators for static and dynamic reactive power support was studied via simulations in [7]. Furthermore, provisioning of reactive power support-based AS was demonstrated in [10] while Dutta et al. [11] developed a scheduling scheme for Volt–VAR devices to control bus voltage magnitude in ADN. An energy storage system (ESSs) planning algorithm was proposed in [12] for providing localized reactive power support, peak shaving, and energy arbitrage related ASs. Guo et al. [13] introduced a coordinated voltage control scheme for ADNs to regulate bus voltages.

These above works are based on centralized optimization approaches, and have demonstrated how to leverage the flexibility of DERs in an ADN for provisioning of ASs. However, as the number of microgrids and smart buildings grows, such centralized techniques would not remain practical and scalable. Specifically, it is neither desirable nor feasible for a single entity to keep track of local generation, demand, state of charge of storage units, load curtailment preferences, and other operational constraints of all constituent smart buildings and microgrids in an ADN to jointly schedule their operation. Increasing concern regarding user privacy is another aspect that may hinder deployment of such centralized schemes.

In contrast with centralized optimization, in distributed optimization schemes, the overall optimization problem is decomposed into smaller problems, each solved by an independent entity with limited peer-to-peer communication among such agents. In such distributed schemes, autonomy of the subsystems is preserved and their local information is not shared with other agents. In addition, such schemes are inherently scalable and fault-tolerant. Due to the above advantages, distributed optimization algorithms have been developed for several problems that arise in power systems; see [14] for an extensive review. More specifically, algorithms based on alternating direction method of multipliers (ADMM) [15], [16] have received a lot of attention by the researchers. ADMM-based distributed optimal power flow (OPF) was investigated in [17] and [18]. A distributed energy management framework employing ADMM was developed in [19] to obtain optimal scheduling of the energy resources in an ADN. Babagheibi et al. [20] used ADMM while solving congestion management problem in ADN with multimicrogrids.

However, to the best of the authors' knowledge, distributed optimization techniques have not been studied in the context of provisioning ASs by ADNs except in a very recently published work [3]. Quan et al. [3] used a distributed particle swarm optimization-based coordination framework, which provides no guarantee of the optimality of solutions. In addition, their study does not provide any supporting results showing the error between centralized and distributed solutions, which is very crucial to adjudge the quality of the distributed algorithm. In this article, we address the above research gap and propose a distributed optimization approach for coordination of multiple microgrids in an ADN for efficient operation and provisioning of ancillary services. Our contributions are summarized below.

1) We formulate a multistage optimization problem where an ADN provides voltage support-based AS while meeting operational constraints including line flow limits, voltage magnitude limits, microgrid inverter limits, and constraints on battery energy storage systems (BESSs) (Section II). Furthermore, we present a set of mixed-integer linear inequalities to capture the set of feasible active and reactive power exchange between the ADN and the transmission network (TN), which ensure penalty-free operation under the passive voltage support scheme proposed by the Belgian TSO [21]. Our proposed

formulation corrects certain inaccuracies present in a similar formulation proposed in [9] where the set of feasible active and reactive power exchange was incorrectly modeled, which would potentially lead to higher penalty and increased load curtailment in the network.

2) An ADMM-based distributed optimization framework is developed in order to solve the above optimization problem in a fully distributed manner following recent works [16], [22], [23] (Section III). Under the proposed scheme, each microgrid determines its BESS charging schedule and load curtailment while the ADN is responsible for constraints pertaining to power flow and AS support. The proposed approach does not require the presence of a centralized entity (unlike past works, such as [24]), and does not require exchange of dual variables among the agents (unlike [18]). In particular, agents are only required to transmit information about active and reactive power exchange between MGs and ADN, which are then used to achieve consensus.[1]

Detailed numerical results, obtained on the IEEE 33-bus distribution test system (Section IV), illustrate the following:

1) how the proposed scheme leverages inverter reactive power control capabilities (managed locally by MGs) for provisioning ASs (power exchange with TN managed by ADN), and comparison with the formulation developed in [9];
2) the effect of ADMM hyperparameters on the convergence rate, and error between centralized and distributed solutions;
3) the scalability of the proposed approach with an increasing number of microgrids and larger test networks (with 69, 136, and 906 buses).

We conclude with a discussion on promising directions for future research in Section V.

II. Problem Formulation

In this section, we develop a multistage optimization problem for optimal operation of an ADN that provides passive voltage support to the TN. Let the number of buses of the ADN be N_b, total number of distribution lines be N_l, and the number of microgrids connected to the ADN be N_m. Each microgrid consists of a BESS, a photovoltaic (PV) generation unit, and local load with possibility of load curtailment. Thus, each microgrid could well represent a smart sustainable building. The prediction horizon for the problem is denoted by N_p. We define the set $[M] := \{1, 2, \ldots, M\}$ for brevity of notation. The decision vector at time $k \in [N_p]$ is defined as

$$\mathbf{x}_k = [P_k, Q_k, P_k^{\text{inj}}, Q_k^{\text{inj}}, V_k^{\text{sq}}, I_k^{\text{sq}}, P_k^{\text{ex}}, Q_k^{\text{ex}}, P_k^{\text{bat}}, P_k^{\text{curt}}, Q_k^{\text{inv}}, E_{k+1}, C_k^{tn}]^\top$$

where $P_k \in \mathbb{R}^{N_l}$ and $Q_k \in \mathbb{R}^{N_l}$ represent the active and reactive power flows in the lines of the ADN, respectively, $P_k^{\text{inj}} \in \mathbb{R}^{N_b}$ and $Q_k^{\text{inj}} \in \mathbb{R}^{N_b}$ denote the active and reactive power injections in the buses of the ADN, respectively, $V_k^{\text{sq}} \in \mathbb{R}^{N_b}$ denotes the square of the magnitude of bus voltages, $I_k^{\text{sq}} \in \mathbb{R}^{N_l}$ is the square of the magnitude of line currents, $P_k^{\text{ex}} \in \mathbb{R}$ and $Q_k^{\text{ex}} \in \mathbb{R}$ denote the active and reactive power exchange with the TN at the substation node (positive value implies import of power from TN and vice versa), respectively, $P_k^{\text{curt}} \in \mathbb{R}^{N_b}$ refers to the load curtailment in the buses, $P_k^{\text{bat}} \in \mathbb{R}^{N_m}$ refers to the power supplied by the BESSs in the microgrids, $Q_k^{\text{inv}} \in \mathbb{R}^{N_m}$ is the reactive power generation/absorption by the inverters located in microgrids, and $E_{k+1} \in \mathbb{R}^{N_m}$ refers to the available energy of BESS in MGs at time $k+1$ after P_k^{bat} is withdrawn. Note that E_1 represents the energy stored at the current interval and is typically known from the state of charge provided by the battery management system (and hence not a decision variable for the proposed optimization problem). Finally, C_k^{tn} is the cost of violating passive voltage constraint, which will be subsequently defined. We now introduce the operational constraints acting on these decision variables. Important notations are summarized in the Nomenclature.

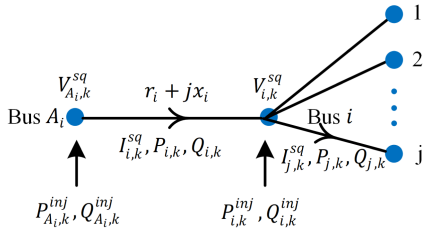

Fig. 1. Notations for branch flow model.

A. Power Flow Constraints

We model the radial ADN using a directed tree graph $\mathcal{S} := (\mathcal{T}, \mathcal{U})$ where $\mathcal{T}$ represents the set of buses and $\mathcal{U}$ is the set of distribution lines. Each bus (or node) i in the graph has a unique ancestor A_i (except the substation node that connects the ADN with the TN), and a set of children nodes denoted by $\mathcal{C}_i$. The convention of graph orientation is such that every line points away from the substation or root node. In Fig. 1, the orientation of the graph is shown where the direction of power flow in line i is assumed to be from the ancestor A_i to the node i. Other quantities, such as nodal injection, line current, and bus voltage, are also shown in the figure.

We have adopted the relaxed branch flow model (also known as *Distflow* model) to represent power flow in the radial ADN [27], [28]. According to [29], branch flow model is more numerically stable than bus injection model. The branch flow equations can be written as

$$P_{i,k} = \sum_{j \in \mathcal{C}_i} (P_{j,k} + I_{j,k}^{\text{sq}} r_j) - P_{i,k}^{\text{inj}}, \quad i \in \mathcal{T} \tag{1a}$$

$$Q_{i,k} = \sum_{j \in \mathcal{C}_i} (Q_{j,k} + I_{j,k}^{\text{sq}} x_j) - Q_{i,k}^{\text{inj}}, \quad i \in \mathcal{T} \tag{1b}$$

$$V_{A_i,k}^{\text{sq}} = V_{i,k}^{\text{sq}} + 2(r_i P_{i,k} + x_i Q_{i,k}) + I_{i,k}^{\text{sq}}(r_i^2 + x_i^2), \quad i \in \mathcal{U} \tag{1c}$$

$$I_{i,k}^{\text{sq}} = \frac{P_{i,k}^2 + Q_{i,k}^2}{V_{i,k}^{\text{sq}}}, \quad i \in \mathcal{U} \tag{1d}$$

[1] An added advantage of our approach is that unlike dual variables that correspond to shadow prices, active and reactive power are physical quantities, and hence less prone to manipulation, which is a growing concern in distributed optimization schemes [25], [26].

where r_j and x_j are the resistance and inductive reactance of the line j, respectively, and $P_{i,k}, Q_{i,k}, P^{\text{inj}}_{i,k}, Q^{\text{inj}}_{i,k}, V^{\text{sq}}_{i,k}$, and $I^{\text{sq}}_{i,k}$ are the ith elements of vectors $P_k, Q_k, P^{\text{inj}}_k, Q^{\text{inj}}_k, V^{\text{sq}}_k$, and I^{sq}_k, respectively. In particular, $P_{i,k}$ and $Q_{i,k}$ are the active and reactive power flow from bus A_i to bus i, respectively, and $P^{\text{inj}}_{i,k}$ and $Q^{\text{inj}}_{i,k}$ are active and reactive power injections at bus i, respectively.

In the above branch flow model, (1a)–(1c) are linear constraints while (1d) is nonlinear and nonconvex in the decision variables. Past work has explored several approaches for obtaining tractable approximations to the nonconvex power flow equations.[2] Inspired by past works, such as [9] and [30], we have considered a linearization of (1d) using first-order Taylor's series approximation around an initial estimate of $I^{\text{sq}}_{i*}(P_{i*}, Q_{i*}, V^{\text{sq}}_{i*})$ given by

$$I^{\text{sq}}_{i,k} = I^{\text{sq}}_{i*} + (P_{i,k} - P_{i*}) \left[\frac{\partial I^{\text{sq}}_{i,k}}{\partial P_{i,k}}\right]_{I^{\text{sq}}_{i*}} + (Q_{i,k} - Q_{i*}) \left[\frac{\partial I^{\text{sq}}_{i,k}}{\partial Q_{i,k}}\right]_{I^{\text{sq}}_{i*}} + (V^{\text{sq}}_{i,k} - V^{\text{sq}}_{i*}) \left[\frac{\partial I^{\text{sq}}_{i,k}}{\partial V^{\text{sq}}_{i,k}}\right]_{I^{\text{sq}}_{i*}}. \tag{2}$$

The solution of the multistage optimization problem obtained at the previous iteration is used as the point of linearization for better accuracy.

The branch power flow limits (thermal limits) for each line in the ADN are given in terms of the maximum apparent power handling capability ($S^{\max}_i$) of the lines. Assuming a relatively high value of branch power flow limit, the limits on active and reactive power flows can be set as

$$-P^{\max}_i \le P_{i,k} \le P^{\max}_i \tag{3a}$$

$$-Q^{\max}_i \le Q_{i,k} \le Q^{\max}_i \tag{3b}$$

where $P^{\max}_i$ and $Q^{\max}_i$ are both set equal to $(S^{\max}_i/\sqrt{2})$. This corresponds to an inner approximation of the circular limit by a square contained entirely within the circle. The voltage limit on buses of the ADN is given by

$$(V^{\min})^2 \le V^{\text{sq}}_{i,k} \le (V^{\max})^2. \tag{4}$$

B. Passive Voltage Support Constraints

In our study, we have considered the Belgian TSO's proposal [21] to penalize distribution system operator (DSO) if the DN is operated beyond the recommended zone, as shown in Fig. 2. According to the proposal in [21], there are the following two zones of operation.

[2]Since the ancillary service requirements imposed by Belgian TSO necessitate introduction of integer variables, which considerably increases the computational burden, we resorted to using linearized power flow equations so that the overall problem remains a mixed-integer linear program (MILP) and the equality constraints remain linear. Algorithms for MILP problems are quite mature with solvers, such as MOSEK, performing extremely well in practice, while mixed-integer nonlinear programming (MINLP) problems are intractable for the most part. In addition, nonconvex equality constraints induced by nonlinear power flow equations scale with the size of the network, and will lead to exponential increase in computation time for larger networks. Therefore, we believe that linearization of power flow equations is essential for the problem studied in this work.

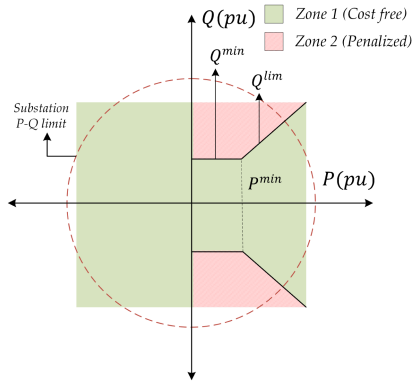

Fig. 2. Passive voltage support curve by Belgian's TSO proposal (*Figure is not drawn to scale*).

1) Zone 1 refers to the region with $\cos(\phi) \ge 0.95$ (ϕ being the power factor) for $P^{\text{ex}}_k \ge P^{\min}$ and the rectangular region formed by $P^{\min}$ and $Q^{\min}$ for $P^{\text{ex}}_k < P^{\min}$ or when ADN is supplying power to the TN. This zone is the cost-free zone and it is desired that the active and reactive power exchange belong to this zone.
2) Zone 2 refers to the region with $\cos(\phi) < 0.95$ for $P^{\text{ex}}_k \ge P^{\min}$ and the zone excluding the rectangular zone formed by $P^{\min}$ and $Q^{\min}$ for $0 \le P^{\text{ex}}_k < P^{\min}$. When the power exchange lies in this zone, the ADN is penalized.

For active power below $P^{\min}$, the reactive power is constrained to be below a certain constant $Q^{\min}$. The cost to the ADN at time k under the passive voltage support scheme is given by

$$C^{\text{tn}}_k := \begin{cases} c^p(|Q^{\text{ex}}_k| - Q^{\text{lim}}), & \text{if } Q^{\text{ex}}_k \text{ belongs to Zone 2} \\ 0, & \text{if } Q^{\text{ex}}_k \text{ belongs to Zone1} \end{cases} \tag{5}$$

where c^p is the penalty factor, and Q^{ex}_k is the reactive power exchange with the TN. Our aim is to represent the above discontinuous cost function in terms of suitable mixed-integer linear constraints that will ensure that the power exchanges lie in Zone 1 (cost-free zone) of Fig. 2.

Remark 1: While the past works [9] also considered the above passive voltage support scheme, their reformulation of the above cost function into mixed-integer linear inequality constraints ([9, eq. (10)]) is incorrect to the best of the authors' knowledge. In particular, considering the value of $Q^{\min}$ as given in [9, Table II], their formulation fails to capture the separating boundary between Zone 1 and Zone 2 for P^{ex} greater than $P^{\min}$ in Fig. 2. Even if we consider any other value of $Q^{\min}$, their formulation fails to capture the rectangular region formed by $P^{\min}$ and $Q^{\min}$ in Fig. 2.

We now propose an alternative mixed-integer reformulation that exactly captures all the intricacies of (5), as shown in Fig. 2. We introduce the following three binary variables:

1) δ^p_k, which takes value 1 when P^{ex}_k is negative and vice versa;
2) δ^{ϕ}_k, which takes value 1 when Q^{ex}_k is within Zone 1 and value 0 when Q^{ex}_k is within Zone 2;
3) δ_k, which takes value 0 when $P^{\text{ex}}_k \ge P^{\min}$ and vice versa.

Consider the following collection of inequalities.

1) The following inequalities:

$$C_k^{tn} \geq 0 \tag{6a}$$

$$C_k^{tn} \leq M^p(1-\delta_k^p) \tag{6b}$$

$$C_k^{tn} \leq M^p(1-\delta_k^\phi) \tag{6c}$$

where M^p is the "Big-M" constant, ensures that the penalty cost for ADN (i.e., C_k^{tn}) is bounded by $[0, M^p]$ if operating point $(P_k^{\text{ex}}, Q_k^{\text{ex}})$ is in Zone 2, otherwise it is zero.

2) Consider the following inequalities:

$$-\left((C_k^{tn}/c^p)+Q^{\text{lim}}+(M^p/c^p)(\delta_k^p+\delta_k^\phi)\right) \leq Q_k^{\text{ex}} \leq (C_k^{tn}/c^p)+Q^{\text{lim}}+(M^p/c^p)(\delta_k^p+\delta_k^\phi) \tag{7a}$$

$$-(M^p\delta_k^\phi - Q^{\text{lim}}) \leq Q_k^{\text{ex}} \leq (M^p\delta_k^\phi - Q^{\text{lim}}) \tag{7b}$$

$$-\left(Q^{\text{lim}}+M^p(1-\delta_k^\phi)+\delta_k^p M^p\right) \leq Q_k^{\text{ex}} \leq Q^{\text{lim}}+M^p(1-\delta_k^\phi)+\delta_k^p M^p. \tag{7c}$$

Equation (7a) bounds C_k^{tn} in $[c^p(|Q_k^{\text{ex}}|-Q^{\text{lim}}), M^p]$ if operating point is in Zone 2, and (7b) and (7c) ensure that Q_k^{ex} is bounded by $[Q^{\text{lim}}, Q^{\text{lim}}+M^p]$ if operating point is in Zone 2.

3) The following inequalities:

$$-(M^p(1-\delta_k)+\zeta) \leq P_k^\mu \tan\phi \leq M^p(1-\delta_k)+\zeta \tag{8a}$$

$$P_k^{\text{ex}} - P_k^\mu \leq \zeta(1-\delta_k)+\delta_k P^{\min} \tag{8b}$$

$$P_k^{\text{ex}} - P_k^\mu \geq -\delta_k M^p \tag{8c}$$

$$P_k^\mu \geq (1-\delta_k)P^{\min} \tag{8d}$$

where ζ is a very small positive constant, define an auxiliary decision variable P_k^μ, which takes value P_k^{ex} if $P_k^{\text{ex}} \geq P^{\min}$, and ζ, otherwise. The P_k^μ is used to capture the linearly increasing Zone 1 of Fig. 2.

4) The separating boundary between Zone 1 and Zone 2 is formed by the following equality constraint:

$$Q^{lim} = \delta_k Q^{\min} + P_k^\mu \tan\phi \tag{9}$$

where Q^{lim} takes value $Q^{\min}$ if P_k^{ex} is below the limit of $P^{\min}$; otherwise, it increases linearly with P_k^{ex}.

5) Finally, the constraints

$$P_k^{\text{ex}} \geq -\delta_k^p M^p \tag{10a}$$

$$P_k^{\text{ex}} \leq M^p(1-\delta_k^p) \tag{10b}$$

ensure that P_k^{ex} is bounded by $[0, M^p]$ or $[-M^p, 0]$ depending on its sign.

The reactive and active power limits $Q^{\min}$ and $P^{\min}$ are defined as

$$-((V_{\text{tr}}/100)S_{\text{tr}}) \leq Q^{\min} \leq (V_{\text{tr}}/100)S_{\text{tr}} \tag{11a}$$

$$P^{\min} = Q^{\min}\cot\phi \tag{11b}$$

where V_{tr} is the substation transformer's short circuit voltage (in %), and S_{tr} is the nominal apparent power of the transformer. The constraint (11) is used to prevent the transformer from becoming disconnected during very lightly loaded condition of DN [8].

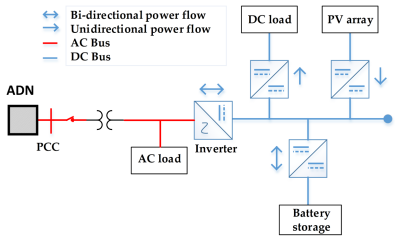

Fig. 3. Schematic of microgrid.

C. Operational Constraints of Microgrids

Each microgrid is equipped with an inverter at the point of interface between ac (load, connection with ADN) and dc (storage, load, and PV units) components (see Fig. 3). Smart inverters now have the capability to provide reactive power support under different modes of operations [31], [32], such as constant power factor mode, voltage reactive power mode, active power–reactive power mode, and constant reactive power mode. The recent development reported in [33] makes it possible to use full capability of inverter without any constraint on operating power factors. Such developments enable inverters to provide purely reactive power that can replace the additional installations of reactive power compensators. In a recent work [8], the authors suggest to use this mode for providing voltage support-based ancillary services. We follow this approach and impose the following constraints on active and reactive power exchange through inverters that interface microgrids to DN:

$$(P_{i,k}^{\text{inv}})^2 + (Q_{i,k}^{\text{inv}})^2 \leq (S_i^{\text{inv}})^2 \quad \forall i \in \mathcal{M} \tag{12}$$

where the set $\mathcal{M}$ holds the bus indices at which microgrids are located, $P_{i,k}^{\text{inv}} := P_{i,k}^{\text{inj}} + P_{i,k}^{\text{load,ac}} - P_{i,k}^{\text{curt}}$ with $P_{i,k}^{\text{load,ac}}$ being the local ac load (refer to Fig. 3), and S_i^{inv} is the maximum allowable apparent power through the inverter at ith bus. Following [9] and [30], we consider the following piecewise linearization of (12) and obtain

$$a_j^p(P_{i,k}^{\text{inv}}) + b_j^q(Q_{i,k}^{\text{inv}}) + c_j \leq 0 \quad \forall i \in \mathcal{M}, j \in [l] \tag{13}$$

where l being the total number of piecewise segments, and

$$a_j^p = 2\sin(\pi/l)\sin(\frac{\pi}{l}(2j-1)) \tag{14a}$$

$$b_j^q = 2\sin(\pi/l)\cos(\frac{\pi}{l}(2j-1)) \tag{14b}$$

$$c_j = -(S_i^{\text{inv}}\sin(2\pi/l)). \tag{14c}$$

Each microgrid considered in our study consists of a BESS, RES (PV array generation), and local load, as shown in Fig. 3. The dynamic operation of energy storage systems is represented as

$$E_{i,k+1} = E_{i,k} - \eta P_{i,k}^{\text{bat}} \tag{15a}$$

$$E_{\min} \leq E_{i,k+1} \leq E_{\max} \tag{15b}$$

$$P_{\min}^{\text{bat}} \leq P_{i,k}^{\text{bat}} \leq P_{\max}^{\text{bat}} \tag{15c}$$

where $k \in [N_p]$, $i \in \mathcal{M}$, and η is the product of BESS's efficiency and sampling time of the optimization problem. $E_{\max}$ and $E_{\min}$ are, respectively, assumed to be 0.9 and 0.2 times the battery capacity. The active and reactive power balance equations for microgrid $i \in \mathcal{M}$ at time $k \in [N_p]$ are given by

$$P^{\text{inj}}_{i,k} = P^{\text{bat}}_{i,k} + P^{\text{pv}}_{i,k} + P^{\text{curt}}_{i,k} - P^{\text{load}}_{i,k} \tag{16a}$$

$$Q^{\text{inj}}_{i,k} = Q^{\text{inv}}_{i,k} + P^{\text{curt}}_{i,k} \tan \Omega_i - Q^{\text{load}}_{i,k} \tag{16b}$$

where $P^{\text{pv}}_{i,k}$ is the PV array generation at the ith microgrid, $P^{\text{load}}_{i,k}$ is the local load (includes both ac and dc load) of ith microgrid, $Q^{\text{load}}_{i,k}$ is the local reactive load of ith microgrid, and Ω_i is load power factor angle at ith microgrid. We assume that reasonably accurate forecast of PV generation and load over the prediction horizon are available to the decision-maker. Note that, load deferment can also be implemented by adding suitable linear constraints as mentioned in [34] with minor changes in the proposed framework.

D. Multistage Optimization Problem

The objective of the ADN is to minimize the total cost, which includes the following:

1) the cost of purchasing active power from the TN, which equals $\beta^p_k P^{\text{ex}}_k$ with β^p_k being the tariff of energy purchase;
2) the penalty due to violating voltage support constraints (i.e., C^{tn}_k);
3) the penalty due to resistive loss in the lines of the ADN, which is defined as $\sum_{l=1}^{N_l} \beta^{\text{loss}}_l I^{\text{sq}}_{l,k} r_l$, where β^{loss}_l is the penalty for energy loss;
4) the operational cost of BESS (i.e., $\sum_{j=1}^{N_m} \beta^b_j P^{\text{bat}}_{j,k}$);
5) the cost due to load curtailment at microgrids, which is defined as $\sum_{j=1}^{N_b} \beta^c_j P^{\text{curt}}_{j,k}$, assuming a reasonable value for penalty factor β^c_k;

over a prediction horizon of length N_p.

Formally, we define

$$C(\mathbf{x}) := \sum_{k=1}^{N_p} \Bigg[\beta^p_k P^{\text{ex}}_k + C^{tn}_k + \sum_{l=1}^{N_l} \beta^{\text{loss}}_l I^{\text{sq}}_{l,k} r_l + \sum_{j=1}^{N_b} \beta^c_j P^{\text{curt}}_{j,k} + \sum_{j=1}^{N_m} \beta^b_j P^{\text{bat}}_{j,k} \Bigg] \tag{17}$$

where $\mathbf{x} := \{\mathbf{x}_k\}_{k\in[N_p]}$ denotes the decision variables over the entire horizon. The above cost can be stated compactly as $\sum_{k=1}^{N_p} c^\top \mathbf{x}_k$, where c is the vector of penalty factors of appropriate dimension. The complete multistage optimization problem can now be stated in a compact form as

$$\min_{\mathbf{x},v} \quad \sum_{k=1}^{N_p} \left[c^\top \mathbf{x}_k \right] \tag{18a}$$

$$\text{s.t.} \quad H_1 \mathbf{x}_k + V v_k + h_1 \le 0 \tag{18b}$$

$$H_2 \mathbf{x}_k + h_2 = 0 \tag{18c}$$

$$G_1 \mathbf{x}_k + g_1 \le 0 \tag{18d}$$

$$G_2 \mathbf{x}_k + g_2 = 0 \tag{18e}$$

where the constraints hold for all $k \in [N_p]$, $v := \{v_k\}_{k\in[N_p]}$ is the vector of binary variables over the entire horizon, H_1, H_2, G_1, G_2, and V are matrices, and h_1, h_2, g_1, and g_2 are vectors of suitable dimensions. Specifically, we encode

1) limits on line flow (3), voltage magnitude (4), and AS support constraints (6a)–(11b) in (18b);
2) linearized power flow (1a)–(1c) and (2) in (18c);
3) inequality constraints pertaining to microgrid inverter and BESSs stated in (13), (15b), and (15c) in (18d);
4) energy and power balance equations from (15a) and (16) in (18e).

Note that, (18b) and (18c) encode constraints pertaining to the entire ADN while (18d) and (18e) represent the constraints that are local to MGs. The above problem is an instance of a MILP. While MILP problems are inherently NP-hard, the number of integer decision variables in (18) is $3N_p$, and does not scale with the size of the network. As a result, it is possible to obtain a globally optimal solution using suitable solvers if N_p is chosen carefully. Further discussions on this issue are presented in Section IV.

III. Proposed Distributed Formulation

We now present a distributed formulation of the above multistage optimization problem (18). We consider a set of $N_m + 1$ agents; one agent responsible for each microgrid and one agent that corresponds to an ADN operator. We define a connected communication graph $\mathcal{G} := (\mathcal{V}, \mathcal{E})$, where $\mathcal{V} := \{0, 1, \ldots N_m\}$ is the set of nodes, which corresponds to the agents, and $\mathcal{E} \subset \mathcal{V} \times \mathcal{V}$ is the set of communication links $(m, n) \in \mathcal{E}$ implying that the agents m and n are connected. While the communication graph can be defined depending on the communication capabilities of the MG nodes, at the very least it is assumed that each MG can communicate with the ADN agent and vice versa.

We now split the decision vector $\mathbf{x}_k$ for the centralized optimization problem (18) as follows. We define $\mathbf{z}_{0,k} := [P_k, Q_k, V^{\text{sq}}_k, I^{\text{sq}}_k, P^{\text{ex}}_k, Q^{\text{ex}}_k, \{P^{\text{inj}}_{j,k}, Q^{\text{inj}}_{j,k}, P^{\text{curt}}_{j,k}\}_{j\notin\mathcal{M}}, C^{tn}_k, v_k]$ to be the decision vector for ADN (agent 0). Similarly, the decision vector for ith MG (agent i) is defined as $\mathbf{z}_{i,k} := [P^{\text{bat}}_{i,k}, P^{\text{curt}}_{i,k}, E_{i,k+1}, Q^{\text{inv}}_{i,k}]$, where $i \in [N_m]$. Note further that it is natural to treat constraints (18d) and (18e) as internal constraints of MGs and constraints (18b) and (18c) as internal constraints of ADN. However, the variables $\{P^{\text{inj}}_{j,k}, Q^{\text{inj}}_{j,k}\}_{j\in\mathcal{M}}$ that correspond to active and reactive power exchange between jth MG and ADN are important for both MGs as well as the ADN to satisfy their internal constraints. Therefore, we define $\mathbf{y}_k := \{P^{\text{inj}}_{j,k}, Q^{\text{inj}}_{j,k}\}_{j\in\mathcal{V}}$ to be shared variables such that each agent maintains a copy of these variables, and the distributed problem is formulated such that agents strive to achieve consensus on these variables in addition to minimizing their local cost.

The costs for the ADN and the ith microgrid at time k are defined as

$$c^\top_{0,k}\mathbf{z}_{0,k} + \bar{c}^\top_{0,k}\mathbf{y}_{0,k} := C^{tn}_k + \sum_{j\in(\mathcal{T}\setminus\mathcal{M})} \beta^c_j P^{\text{curt}}_{j,k} + \sum_{l=1}^{N_l} \beta^{\text{loss}}_l I^{\text{sq}}_{l,k} r_l + \beta^p_k \left(P^{\text{ex}}_k - \sum_{j\in\mathcal{M}} P^{\text{inj}}_{j,k} \right) \tag{19a}$$

$$c_i^\top \mathbf{z}_{i,k} + \bar{c}_{i,k}^\top \mathbf{y}_{i,k} := \beta_i^c P_{i,k}^{\text{curt}} + \beta_i^b P_{i,k}^{\text{bat}} + \beta_k^p P_{i,k}^{\text{inj}}. \tag{19b}$$

In other words, the sum of local costs of the ADN and each microgrid over the horizon coincides with the total cost of the centralized problem stated in (17) when agents reach consensus over the shared variables. The above definition implies that the ADN is responsible for minimizing the cost of active power consumption at all nodes that do not have an MG while each MG is responsible for its own active power consumption cost. Both ADN and the MGs evaluate the active power consumption cost at the price set by the TSO.

Following similar formulation in [23], the problem in (18) can be equivalently stated as

$$\min_{\substack{\mathbf{z}_0,\mathbf{y}_0 \\ \{\mathbf{z}_i,\mathbf{y}_i\}_{i\in[N_m]}}} \quad \sum_{k=1}^{N_p} \Bigg[c_{0,k}^\top \mathbf{z}_{0,k} + \bar{c}_{0,k}^\top \mathbf{y}_{0,k} + \sum_{i=1}^{N_m} (c_i^\top \mathbf{z}_{i,k} + \bar{c}_{i,k}^\top \mathbf{y}_{i,k}) \Bigg] \tag{20a}$$

$$\text{s.t.} \quad A_1 \mathbf{z}_{0,k} \le d_1 \tag{20b}$$

$$A_0 \mathbf{z}_{0,k} + B_0 \mathbf{y}_{0,k} = d_0 \tag{20c}$$

$$F_i \mathbf{z}_{i,k} + B_i \mathbf{y}_{i,k} \le f_i \quad \forall i \in [N_m] \tag{20d}$$

$$\mathbf{y}_{m,k} = u_{mn,k} \quad \forall m \in \mathcal{V},\ (m,n) \in \mathcal{E} \tag{20e}$$

$$\mathbf{y}_{n,k} = u_{mn,k} \quad \forall n \in \mathcal{V},\ (m,n) \in \mathcal{E} \tag{20f}$$

where the constraints hold for every $k \in [N_p]$. We include the constraints in (18b) in terms of (20b), (20c) corresponds to (18c), (18d) and (18e) are merged into (20d), and auxiliary variables $u_{mn,k}$ enforce consensus constraints over shared variables between two neighboring agents m and n of the communication graph.

We leverage the fully distributed ADMM algorithm from [16] and [23] to solve the above problem stated in (20). The complete algorithm is stated in Algorithm 1. We denote by $\lambda_{i,k} \in \mathbb{R}^p$ the Lagrange multipliers corresponding to the equality constraints in (20e) and (20f). The optimization subproblem for the ADN using the augmented Lagrangian function is defined as

$$\min_{\mathbf{z}_0,\mathbf{y}_0} L_\rho(\mathbf{z}_0, \mathbf{y}_0, \lambda_0, \{\mathbf{y}_m\}_{m\in\mathcal{N}_0}) = \sum_{k=1}^{N_p} \Bigg[c_{0,k}^\top \mathbf{z}_{0,k} + \bar{c}_{0,k}^\top \mathbf{y}_{0,k} + \mathbf{y}_{0,k}^\top \lambda_{0,k} + (\rho/2) \sum_{m\in\mathcal{N}_0} \left\| \mathbf{y}_{0,k} - \frac{\widehat{\mathbf{y}}_{0,k} + \mathbf{y}_{m,k}}{2} \right\|_2^2 \Bigg] \tag{21a}$$

$$\text{s.t.} \quad A_0 \mathbf{z}_{0,k} + B_0 \mathbf{y}_{0,k} = d_0 \tag{21b}$$

$$A_1 \mathbf{z}_{0,k} \le d_1 \quad \forall k \in [N_p] \tag{21c}$$

where the ADN agent uses the shared variables $\mathbf{y}_{m,k}$ received from its neighbors $\mathcal{N}_0$ and its local copy of the shared variables obtained in the previous iteration $\widehat{\mathbf{y}}_{0,k}$ in the second term of the augmented Lagrangian to achieve consensus with its neighbors. The hyperparameter ρ controls the relative weight of the consensus term and the cost terms in the cost function of (21). The Lagrange multipliers are updated locally by the ADN agent as shown in Line 4 of Algorithm 1. The above problem is an instance of a mixed-integer quadratic program (MIQP).

Algorithm 1: Fully Distributed ADMM.

1 **Initialization:** At $t = 0$, $\mathbf{y}_j^t = y_0 \in \mathbb{R}^p$ and $\lambda_j^t = 0$ for any $j \in \mathcal{V}$,
2 **while** $\max_{j\in\mathcal{V}} \left\| \mathbf{y}_j^t - \frac{1}{|\mathcal{N}_j|} \sum_{l\in\mathcal{N}_j} [\mathbf{y}_l^t] \right\|_2^2 \ge \epsilon$ **do**
3 **for** $j \in |\mathcal{V}|$ **do**
4 $\lambda_j^{t+1} \leftarrow \lambda_j^t + \rho \sum_{m\in\mathcal{N}_j} (\mathbf{y}_j^t - \mathbf{y}_m^t)$
5 $(\mathbf{z}_j^{t+1}, \mathbf{y}_j^{t+1}) \leftarrow$ $\arg\min_{(\mathbf{z}_j^t,\mathbf{y}_j^t)\in\mathcal{S}} L_\rho(\mathbf{z}_j^t, \mathbf{y}_j^t, \lambda_j^{t+1}, \{\mathbf{y}_l^t\}_{l\in\mathcal{N}_j})$
6 communicate $\mathbf{y}_j^{t+1}$ to neighbors in $\mathcal{N}_j$
7 set $\widehat{\mathbf{y}}_j \leftarrow \mathbf{y}_j^{t+1}$
8 **end**
9 $t \leftarrow t + 1$
10 **end**
11 **Output:** $\{\mathbf{y}_j^t, \mathbf{z}_j^t\}$ for any $j \in \mathcal{V}$.

We now state the subproblem for ith MG below:

$$\min_{\mathbf{z}_i,\mathbf{y}_i} L_\rho(\mathbf{z}_i, \mathbf{y}_i, \lambda_i, \{\mathbf{y}_m\}_{m\in\mathcal{N}_i}) = \sum_{k=1}^{N_p} \Bigg[c_i^\top \mathbf{z}_{i,k} + \bar{c}_{i,k}^\top \mathbf{y}_{i,k} + \mathbf{y}_{i,k}^\top \lambda_{i,k} + (\rho/2) \sum_{m\in\mathcal{N}_i} \left\| \mathbf{y}_{i,k} - \frac{\widehat{\mathbf{y}}_{i,k} + \mathbf{y}_{m,k}}{2} \right\|_2^2 \Bigg] \tag{22a}$$

$$\text{s.t.} \quad F_i \mathbf{z}_{i,k} + B_i \mathbf{y}_{i,k} \le f_i \quad \forall k \in [N_p] \tag{22b}$$

where $\mathcal{N}_i$ is the set of neighbors for ith agent, and ρ is the penalty factor for the quadratic regularizer term. The above problem is an instance of a quadratic program.

Each agent solves its own subproblem, and communicates the individual copy of the shared variable vector $\mathbf{y}_k$ with every other agent at each iteration t following the ADMM algorithm. The distributed operation is depicted in Fig. 4 where microgrid agents $m \in \mathcal{V} \setminus \{0\}$, and $n \in \mathcal{V} \setminus \{0\}$ with all possible pairs of $(m,n) \in \mathcal{E}$, and $m \ne n$ share their copy of shared variable vectors ($\mathbf{y}_m$ and $\mathbf{y}_n$, respectively) between each other as well as with the ADN agent. The ADMM generates primal–dual sequences as $\{\mathbf{z}_{j,k}, \mathbf{y}_{j,k}\}$ and $\{\lambda_{j,k}\}$ that get updated with every iteration t following the Algorithm 1. The algorithm terminates when the local copy of the shared variable maintained by the agents becomes approximately equal to the average of the shared variables received from their neighbors up to a tolerance parameter ϵ (see Line 2 in the Algorithm).

Remark 2: The algorithm presented above has been demonstrated to converge to the centralized optimal solution in convex finite-sum settings in [16]. However, the subproblem of the ADN agent in (21) takes the form of mixed-integer quadratic programming, for which theoretical convergence guarantees are not known. Nevertheless, convergence of ADMM-based algorithms, where the centralized problem is an MILP, has been empirically observed in power systems applications [35], [36], [37]. In the following section, we present a thorough empirical

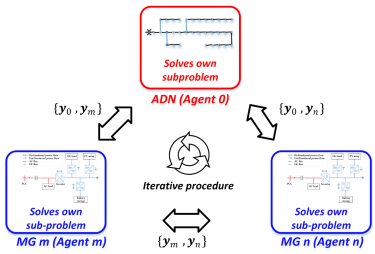

Fig. 4. Schematic of distributed operation.

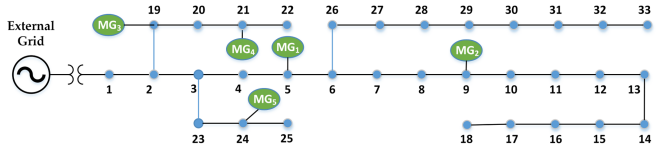

Fig. 5. Modified IEEE 33-bus DN.

analysis of the convergence of Algorithm 1 for different choice of hyperparameters and network sizes.

Remark 3: In contrast with other ADMM-based distributed optimization formulations, such as the ones studied in [18], [38], and [39], the above approach requires agents to only communicate a subset of the primal decision variables that are relevant for other agents. Since the primal decision variables correspond to active and reactive power signals, a malicious agent cannot easily tamper with it and leads the distributed scheme to arrive at a solution that is favorable to itself instead of the social optimal solution. In our scheme, dual variables ($\lambda^t_{j,k}$), i.e., shadow price signals, are locally updated by each agent and not shared among neighbors.

IV. Numerical Results

A. Simulation Setup

To validate our proposed formulation, a modified IEEE 33-bus [40] DN (see Fig. 5) is considered for numerical simulation. Five microgrids are added to nodes 5, 9, 19, 21, and 24, respectively. Each microgrid is equipped with local PV generation, local load, storage, and inverter, as shown in Fig. 3. Each agent (the ADN as well as the microgrids) is assumed to be able to communicate with every other agent (i.e., the underlying communication graph is a complete graph). The necessary simulation parameters and system information are provided in Table I and are chosen to simulate the desired behavior of the agents in the scope of the optimization (as in [9]). The cost and penalty parameters are chosen to maintain consistency with the peak tariff rate, as shown in Fig. 6(d).

For the optimization problem, Python-based package Pyomo [41] is used as modeling language, and MOSEK [42] is used as a solver with default settings. Numerical simulation is performed on a Desktop Computer with 2.90 GHz Intel core-i7 processor and 64-GB RAM configurations. We choose a sampling time of 15 min and solve each multistage distributed optimization problem [(21) and (22)] following Algorithm 1 over an entire day in a receding horizon manner (popularly known as model predictive control) [43] with prediction horizon $N_p = 10$.

TABLE I
System Information and Simulation Parameters

Parameter	Symbol	Value
Prediction horizon	N_p	10
Rated DN voltage	V_{rated}	12.66 kV
BESS's capacity	-	600 kWh
Coefficient of BESS's dynamic model	η	0.225 h
PV plant rated power	$P_{\text{pv ,peak}}$	400 kW
Branch flow limit	$S^{\max}$	1200 kVA
Active power limit in Fig. 2	$P^{\min}$	$0.5\times$ (peak exchange)
Reactive power limit in Fig. 2	$Q^{\min}$	$0.33P^{\min}$
Inverters capacity	S^{inv}	250 kVA
Maximum charging/ discharging power of BESS	$P^{\text{bat}}_{\max/\min}$	$(+/-)100$ kW
Piece-wise segments in (13)	l	16
Large constant of Big-M method	M^p	10000
Cost of BESS power utilization	β^b	0.1519 €/kWh
Penalty due to load curtailment	β^c	0.506 €/kWh
Penalty due to line loss	β^{loss}	0.075 €/kWh
Penalty in zone 2 of Fig. 2	c^p	5 €/kVAR
Power factor of AC load in i-th microgrid	$\cos(\Omega_i)$	0.8

The primary motivation for considering a receding horizon approach is the presence of storage systems in the ADN. If we only optimize the instantaneous cost, then the optimal solution will prioritize use of stored energy (which is cheap), while disregarding its future availability. Such an outcome is unacceptable since it is pertinent to store energy during intervals of excess PV generation and low electricity price so as to make use of them during intervals of power scarcity or high price. As a result, formulating a multistage optimization problem is necessary. Within the class of multistage optimization, a receding horizon approach allows us to choose a potentially smaller prediction horizon, and repeatedly refine our solution in an online manner as uncertain parameters, such as PV generation and load, get realized. A smaller N_p also reduces the computational requirement in a considerable manner (compared with a day ahead formulation) since the number of integer variables scales linearly with N_p.

B. Provisioning of Passive Voltage Support as Scheme

As mentioned in Section II, we have considered passive voltage support scheme according to the guidelines given by Belgian TSO. For this simulation, we have considered the load profile data of Belgium area and day-ahead price by Belgian TSO [44] for 22 May, 2022, as shown in Fig. 6(d). In Fig. 6(d), the active power exchange with TN is shown under the implementation of passive voltage support scheme.

The effectiveness of the proposed distributed scheme in providing passive voltage support is shown in Fig. 6(a) at four critical time stamps of 24-h operation period. Time stamp (a) refers to early morning (around 04:00 h) when ADN is lightly loaded, time stamp (b) refers to morning (around 10:00 h) when system load is ramping up to peak, time stamp (c) refers to afternoon (around 15:00 h) when there is relatively less load on

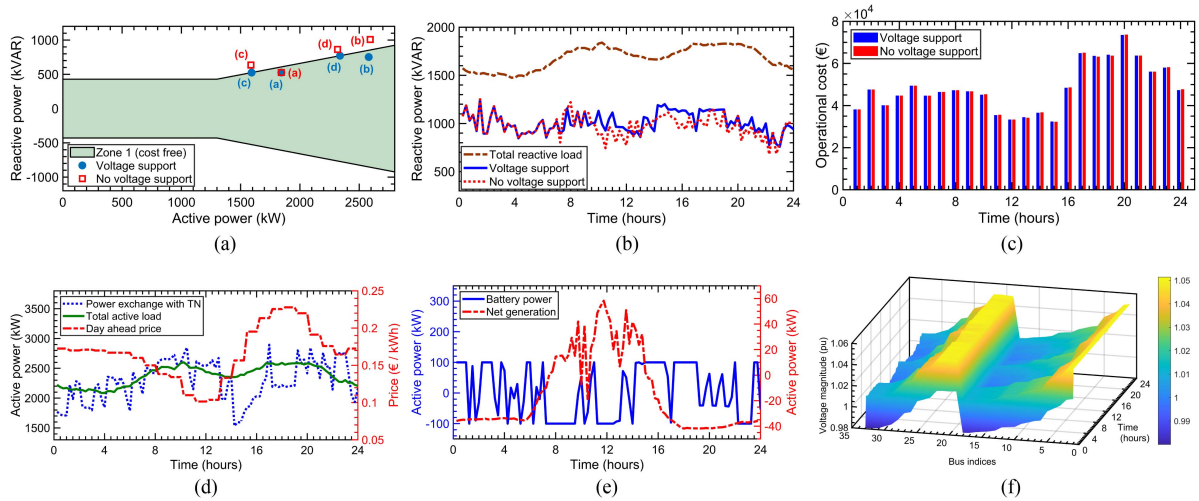

Fig. 6. (a) Passive voltage support curve, (b) total reactive load of DN and aggregated reactive power generation by all inverters both with and without voltage support AS constraints, (c) comparison of operational cost (total operational cost under voltage support is 1 162 460.52 € and without voltage support is 1 162 927.08 €), (d) active power exchange between TN and DN, total active load of DN, and day ahead price by Belgian TSO [44], (e) net generation (PV generation subtracted by local load) in MG 1 and charging/ discharging power of BESS (positive value implies discharging and vice versa), and (f) true bus voltages (solution retrieved from Newton–Raphson load flow) throughout 24-h operation.

the system and lastly, time stamp (d) refers to evening (around 21:00 h) when the load is ramping down from peak. In all of the time zones, our formulation for passive voltage support scheme ensures that active and reactive power exchange with TN remains in penalty-free Zone 1. In contrast, the points under "No voltage support" tag in Fig. 6(a) move to Zone 2 for time stamps (b)–(d) when the passive voltage support constraints are absent despite the inverters being operated with full capability.

The amount of reactive power drawn from TN is significantly smaller compared with the reactive load consumption by ADN. This is due to the fact that we have exploited the full capabilities of inverters, as mentioned in Section II, and these inverters aid in provisioning of ancillary services by supplying additional reactive power for those time stamps where system operation might have shifted to Zone 2. For instance, in the absence of passive voltage support constraints, Fig. 6(b) shows that inverters provide relatively lower amount of reactive power at time stamps (b), (c), and (d) [as shown in Fig. 6(a)] leading to greater demand from TN and consequent operation in Zone 2. When passive voltage support constraints are introduced in the optimization problem, a smaller amount of reactive power is drawn from the grid leading to system operation in the penalty-free Zone 1 [as shown in Fig. 6(a)]. This is corroborated in Fig. 6(b), which shows that a larger amount of reactive power was supplied by the inverters during those time periods.

In terms of operational cost, we observe in Fig. 6(c) that compliance of passive voltage support scheme yields almost same daily operational cost as the "No voltage support" counterpart. In particular, the calculation of operational cost includes the following:

1) the cost of purchasing active power from TSO using the time-varying tariff rates [shown in Fig. 6(d)];
2) the cost of load curtailment;
3) cost of renewable energy from PV plants in MGs.

Operational cost of BESSs is not considered as it is negligible for 24-h operation. In order to obtain a fair comparison, cost due to violation of voltage support constraints is not included since this term was not present in the optimization problem of the "No voltage support" counterpart. However, the net incurred penalty due to operation in Zone 2 under "No voltage support" counterpart comes to 689 514.2 € (considering the value of c^p in Table I borrowed from [9]), whereas the penalty under voltage support constraints is 0 under our proposed formulation. These results show the feasibility of implementing such voltage support schemes without incurring much additional operational cost while entirely avoiding penalty due to operation in Zone 2. Fig. 6(e) shows that BESSs draw power from ADN while the price is relatively low and discharge as the price increases to compensate internal load consumption of MG and ADN.

1) Bus Voltage Profiles: Due to the linearization of nonlinear constraint (1d) into (2), the true voltage magnitudes of nodes may deviate from voltages retrieved as solution of the distributed algorithm. Therefore, at every interval, voltage magnitudes are calculated by conducting Newton–Raphson load flow, which computes voltages using the power injections at the nodes for that particular interval. These true voltages are plotted in Fig. 6(f) for all the buses over the 24-h operation, and are found to be within $\pm 5\%$ of the rated value.

C. Comparison of Our Proposed Method with [9]

In Fig. 7, we compare the solutions obtained under our proposed formulation of the passive voltage support scheme with the formulation presented in [9]. It is evident from the figure that under the constraints presented in [9], the reactive power exchange at the optimal solutions is restricted to $Q^{\min}$ as explained in Remark 1 of Section II. Furthermore, in order to guarantee penalty-free operation, the optimal solution obtained under the formulation given in [9] needs to increase load curtailment by 5.31% of the total load compared with no curtailment of load observed under our proposed scheme.

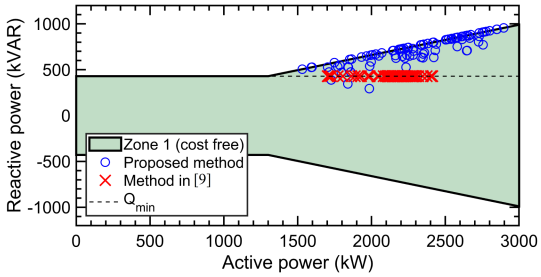

Fig. 7. Comparison with [9].

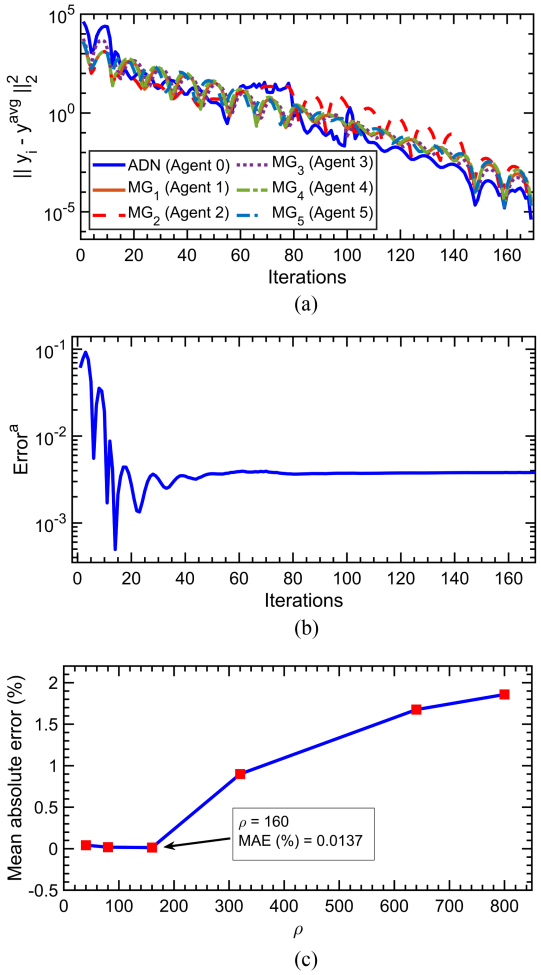

Fig. 8. (a) Convergence of shared variable y_i^t (when $\rho = 160$ and $\epsilon = 10^{-4}$), (b) convergence of error in optimal costs between centralized and distributed solutions (Error^a), and (c) Error^b with varying ρ (when $\epsilon = 10^{-4}$).

D. Convergence Behavior of the Distributed Algorithm

We now examine the convergence behavior of the distributed optimization formulation and provide detailed insights into how to choose different hyperparameters while deploying such schemes in practice. The earlier test bed, i.e., the modified IEEE 33-bus ADN with five MGs (as shown in Fig. 5) is chosen for this study as well. Prediction horizon for each subproblem is kept at 10.

Fig. 8(a) depicts the convergence of shared variables $\mathbf{y}_i^t$ for each agent to the average $\mathbf{y}^{\text{avg}}$ value and shows that consensus among all agents is achieved for a given tolerance (as given in line 2 of Algorithm 1). In Fig. 8(b), we also show the convergence of the error in optimal cost between centralized and distributed solution, which is defined as

$$\text{Error}^a = \frac{\mid C(\mathbf{x}^\star) - \{\hat{c}_0 + \sum_{i=1}^{N_m} \hat{c}_i\} \mid}{\mid C(\mathbf{x}^\star) \mid} \tag{23}$$

where $C(\mathbf{x}^\star)$ is the optimal cost (17) under centralized solution, $\hat{c}_0 := \sum_{k=1}^{N_p} [c_{0,k}^\top \mathbf{z}_{0,k} + \bar{c}_{0,k}^\top \mathbf{y}_{0,k}]$ is defined from (21a) and $\hat{c}_i := \sum_{k=1}^{N_p} [c_i^\top \mathbf{z}_{i,k} + \bar{c}_{i,k}^\top \mathbf{y}_{i,k}]$ is defined from (22a). Error^a is plotted in log scale and is found to be converging quickly. We also compute the error between the shared variables y_i obtained from the solution of the distributed algorithm and the centralized solution [as given in (18)]. This mean absolute error is defined as

$$\text{Error}^b = \left[\frac{1}{(N_m+1).N_{\text{sh}}}\right] \sum_{i=1}^{N_m+1} \sum_{j=1}^{N_{sh}} \frac{\mid y_j^{\text{cent}} - y_{i,j} \mid}{\mid y_j^{\text{cent}} \mid} \tag{24}$$

where y_j^{cent} is the jth element of the shared variable vector y^{cent}, which can be obtained from (18), $y_{i,j}$ is the jth element of y_i vector that belongs to ith agent, and N_{sh} is the total number of shared variables. The Error^b is shown in Fig. 8(c) for different values of hyperparameter ρ. The ADMM scheme terminates when the consensus error becomes smaller than tolerance $\epsilon = 10^{-4}$ for each agent as given in line 2 of Algorithm 1. The smallest deviation between the centralized and distributed solutions (i.e., Error^b) is obtained when $\rho = 160$ with the mean absolute error being 0.0137%.

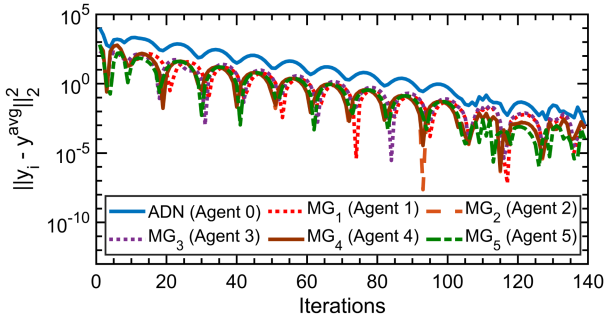

Fig. 9. Convergence of shared variable y_i^t (when $\epsilon = 10^{-4}$) for European low-voltage test feeder network of 906 buses.

TABLE II
ANALYSIS OF COMPUTATIONAL TIME FOR AGENTS

Tolerance (ϵ)	Value of ρ	Iterations	Computation time per iteration (s)		Error^a (%)
			ADN	MG	
10^{-2}	60	122	6.48	0.63	0.2268
	140	114	5.6	0.63	0.2236
	300	109	5.2	0.64	0.2255
	500	102	4.85	0.64	0.1004
10^{-3}	60	151	5.89	0.64	0.2267
	140	137	5.21	0.64	0.2238
	300	132	4.97	0.63	0.2255
	500	121	4.78	0.63	0.1777
10^{-4}	60	174	5.63	0.64	0.2239
	140	170	5.11	0.64	0.2239
	300	163	4.81	0.63	0.2257
	500	154	4.51	0.63	0.2254

TABLE III
COMPUTATION TIME FOR DIFFERENT NETWORK SIZES

Test system	No. of MGs	Iterations	Computation time per iteration (s)		Error[b] (%)
			ADN	MG	
IEEE 33-bus ($N_p = 10$)	5	156	4.16	0.63	0.96
	7	169	4.65	0.82	0.77
	10	197	4.62	0.99	1.22
IEEE 69-bus ($N_p = 10$)	5	135	17.77	0.61	1.11
	7	181	15.49	0.84	1.21
	10	246	13.77	1.13	1.76
136-bus DN ($N_p = 10$)	5	126	14.41	0.927	0.007
	7	175	13.414	1.09	0.01
	10	196	13.79	1.43	0.014
ELV 906-bus ($N_p = 2$)	5	140	25.106	0.205	0.0145
	10	180	26.681	0.1	0.824
	20	259	25.75	0.173	1.39

The per iteration computation time for ADN and MG local optimization problems and the number of iterations required for convergence of ADMM are given in Table II for different values of ρ and error tolerance ϵ. Note that, computational time under the heading "MG" in Table II refers to the mean computational time per iteration required by each MG. It is observed that computational time and number of iterations are smaller for higher values of ρ, i.e., the agents quickly reach consensus on the shared variables. Although Error[a] roughly remains same, increase in ρ leads to a larger mean absolute error (Error[b]) between distributed and centralized solutions [as shown in Fig. 8(c)]. Therefore, users need to choose the value of ρ carefully by evaluating the tradeoff between faster convergence and greater accuracy. Table II provides much valuable insights to this end.

Similarly, smaller ϵ led to a larger number of iterations before convergence is achieved. For the problem considered in this work, value of ρ between 100 and 200 and $\epsilon = 10^{-4}$ led to mean absolute error (Error[b]) being less than 2%. Finally, we clarify that the results given in Table II are to illustrate the relative impact of different parameters, such as ϵ and ρ, on the number of iterations and computation time. The absolute value of computation time would depend on the choice of processor, choice of MILP algorithm, implementation framework, among others; specifically, a native C/C++ implementation would lead to a smaller computation time.

E. Scalability of the Proposed Approach

To investigate the scalability of our formulation, we have carried out additional simulations on the IEEE 69-bus [45] DN, 136-bus DN, and European low-voltage test feeder 906-bus [46] DN. In addition, all the distribution systems are further populated with an increasing number of MGs. Table III gives the number of iterations and per iteration computation time required by the agents to achieve convergence. In addition, the Error[b] between the centralized and distributed solutions is also shown. To accelerate the convergence process with a larger DN, we have chosen penalty factor $\rho = 160$ upto the point when tolerance (ϵ) reaches 10^{-2}, and thereafter, ρ is increased to 1000 until tolerance (ϵ) reaches 10^{-4}.

The table gives that the number of iterations increases as number of MGs grows, primarily due to the increase in the dimension of the shared variables over which agents must achieve consensus. Despite this, the per iteration computation time of the MGs remains relatively same, as the size of the subproblem (22) remains unchanged. However, a notable increase in per iteration computation time for ADN is observed when transitioning to larger networks (where $N_p = 10$), as the size of the subproblem (21) significantly expands due to increase in power flow constraints and line flow limits. The increase is polynomial in nature since there is no increase in the dimension of the integer variables with increase in the network size. In addition, while the subproblem (22) is a quadratic programming instance, the subproblem (21) of ADN belongs to the MIQP category. As a consequence, the solver MOSEK inherently requires more time to solve it. For the 69-bus case, the per iteration computation time of ADN subproblem is relatively higher (even close to 136-bus case) because the feasibility set of (21) resulted in activation of majority number of integer variables (out of $3N_p$), which in turn necessitates MOSEK to solve more number of problems out of total 2^{3N_p} problems.

The total computation time for the European low-voltage test feeder (906-bus) DN was found to be significantly larger. In order to alleviate the computational burden, we reduced N_p from 10 to 2 to reduce the dimension of integer variables in the optimization problem. This resulted in a significant acceleration of per iteration computation time for ADN, which is evident from the table. Fig. 9 shows the convergence behavior of the distributed framework for this 906-bus network with five microgrids.

V. CONCLUSION

In this article, an ADMM-based fully distributed optimization framework is proposed to coordinate multi-MGs in an ADN and provide AS to the TN while satisfying the operational constraints of the network. We presented detailed numerical results on a benchmark DN and showed that participating in the passive voltage support scheme does not lead to any significant increase in the operational cost of the ADN. The effect of ADMM hyperparameters on convergence time and accuracy is thoroughly investigated. The computation time for the ADN and MG subproblems and the impact of network size and prediction horizon are also reported, demonstrating the scalability of our approach.

While passive voltage support-based ancillary service, as recommended by the Belgian TSO, is investigated in this work, the proposed formulation is easily amenable to other types of ancillary services (for instance, Swiss TSO model [8]) as well. Similarly, active voltage support schemes are also realizable in the proposed framework, and will be examined in a follow-up work. In addition, designing distributed algorithms that incorporate the effect of uncertainty associated with renewable energy generation and enable peer-to-peer trading among microgrids while providing ancillary services remains as promising directions for future research. Finally, developing distributed variants of algorithms, such as particle swarm optimization, for constrained multiagent optimization problems that arise in power systems applications should be investigated in future work.

REFERENCES

[1] T. B. Kumar and A. Singh, "Ancillary services in the Indian power sector–A look at recent developments and prospects," *Energy Policy*, vol. 149, 2021, Art. no. 112020.

[2] P. Gautam, P. Piya, and R. Karki, "Resilience assessment of distribution systems integrated with distributed energy resources," *IEEE Trans. Sustain. Energy*, vol. 12, no. 1, pp. 338–348, Jan. 2021.

[3] H. Quan, K. Utkarsh, and D. Srinivasan, "A distributed dual-optimization framework for ancillary-service coordination between MV microgrids and LV distribution networks," *IEEE Syst. J.*, vol. 17, no. 1, pp. 212–223, Mar. 2023.

[4] B. M. Sanandaji, T. L. Vincent, and K. Poolla, "Ramping rate flexibility of residential HVAC loads," *IEEE Trans. Sustain. Energy*, vol. 7, no. 2, pp. 865–874, Apr. 2016.

[5] A. S. Al-Bukhaytan, A. T. Al-Awami, A. M. Muqbel, and F. Al-Ismail, "Dynamic planning of active distribution network's wire and nonwire alternatives considering ancillary services market participation," *IEEE Syst. J.*, vol. 17, no. 2, pp. 2993–3004, Jun. 2023.

[6] H. Karbouj and Z. H. Rather, "Voltage control ancillary service from wind power plant," *IEEE Trans. Sustain. Energy*, vol. 10, no. 2, pp. 759–767, Apr. 2019.

[7] A. O. Rousis, D. Tzelepis, Y. Pipelzadeh, G. Strbac, C. D. Booth, and T. C. Green, "Provision of voltage ancillary services through enhanced TSO-DSO interaction and aggregated distributed energy resources," *IEEE Trans. Sustain. Energy*, vol. 12, no. 2, pp. 897–908, Apr. 2021.

[8] S. Karagiannopoulos, C. Mylonas, P. Aristidou, and G. Hug, "Active distribution grids providing voltage support: The Swiss case," *IEEE Trans. Smart Grid*, vol. 12, no. 1, pp. 268–278, Jan. 2021.

[9] I.-I. Avramidis, F. Capitanescu, V. A. Evangelopoulos, P. S. Georgilakis, and G. Deconinck, "In pursuit of new real-time ancillary services providers: Hidden opportunities in low voltage networks and sustainable buildings," *IEEE Trans. Smart Grid*, vol. 13, no. 1, pp. 429–442, Jan. 2022.

[10] T. Harighi, A. Borghetti, F. Napolitano, and F. Tossani, "Provision of reactive power services by energy communities in MV distribution networks," *Sustain. Energy, Grids Netw.*, vol. 34, 2023, Art. no. 101038.

[11] A. Dutta, S. Ganguly, and C. Kumar, "Coordinated control scheme for EV charging and Volt/VAR devices scheduling to regulate voltages of active distribution networks," *Sustain. Energy, Grids Netw.*, vol. 31, 2022, Art. no. 100761.

[12] H. Abdeltawab and Y. A.-R. I. Mohamed, "Energy storage planning for profitability maximization by power trading and ancillary services participation," *IEEE Syst. J.*, vol. 16, no. 2, pp. 1909–1920, Jun. 2022.

[13] Y. Guo, Q. Wu, H. Gao, X. Chen, J. Østergaard, and H. Xin, "MPC-based coordinated voltage regulation for distribution networks with distributed generation and energy storage system," *IEEE Trans. Sustain. Energy*, vol. 10, no. 4, pp. 1731–1739, Oct. 2019.

[14] D. K. Molzahn et al., "A survey of distributed optimization and control algorithms for electric power systems," *IEEE Trans. Smart Grid*, vol. 8, no. 6, pp. 2941–2962, Nov. 2017.

[15] S. Boyd, N. Parikh, E. Chu, B. Peleato, and J. Eckstein, "Distributed optimization and statistical learning via the alternating direction method of multipliers," *Found. Trends Mach. Learn.*, vol. 3, no. 1, pp. 1–122, 2011.

[16] A. Makhdoumi and A. Ozdaglar, "Convergence rate of distributed ADMM over networks," *IEEE Trans. Autom. Control*, vol. 62, no. 10, pp. 5082–5095, Oct. 2017.

[17] T. Erseghe, "Distributed optimal power flow using ADMM," *IEEE Trans. Power Syst.*, vol. 29, no. 5, pp. 2370–2380, Sep. 2014.

[18] Q. Peng and S. H. Low, "Distributed optimal power flow algorithm for radial networks, I: Balanced single phase case," *IEEE Trans. Smart Grid*, vol. 9, no. 1, pp. 111–121, Jan. 2018.

[19] A. Rajaei, S. Fattaheian-Dehkordi, M. Fotuhi-Firuzabad, M. Moeini-Aghtaie, and M. Lehtonen, "Developing a distributed robust energy management framework for active distribution systems," *IEEE Trans. Sustain. Energy*, vol. 12, no. 4, pp. 1891–1902, Oct. 2021.

[20] M. Babagheibi, S. Jadid, and A. Kazemi, "Distribution locational marginal pricing for congestion management of an active distribution system with renewable-based microgrids under a privacy-preserving market clearing approach and load models," *Sustain. Energy, Grids Netw.*, vol. 32, 2022, Art. no. 100935.

[21] "Study on the future design of the ancillary service of voltage and reactive power control," Belg. Transmiss. System Operator (Elia), 2018. [Online]. Available: https://www.elia.be/-/media/project/elia/elia-site/electricity-market-and-system---document-library/voltage-services---vsp-and-reactive-power-management/2018/2018-design-note-future-voltage-and-reactive-power-control.pdf

[22] G. Banjac, F. Rey, P. Goulart, and J. Lygeros, "Decentralized resource allocation via dual consensus ADMM," in *Proc. Amer. Control Conf.*, 2019, pp. 2789–2794.

[23] A. Cherukuri, A. Zolanvari, G. Banjac, and A. R. Hota, "Data-driven distributionally robust optimization over a network via distributed semi-infinite programming," in *Proc. IEEE 61st Conf. Decis. Control*, 2022, pp. 4771–4775.

[24] W. Liu, J. Zhan, and C. Chung, "A novel transactive energy control mechanism for collaborative networked microgrids," *IEEE Trans. Power Syst.*, vol. 34, no. 3, pp. 2048–2060, May 2019.

[25] S. Sundaram and B. Gharesifard, "Distributed optimization under adversarial nodes," *IEEE Trans. Autom. Control*, vol. 64, no. 3, pp. 1063–1076, Mar. 2019.

[26] T. Tanaka, F. Farokhi, and C. Langbort, "Faithful implementations of distributed algorithms and control laws," *IEEE Trans. Control Netw. Syst.*, vol. 4, no. 2, pp. 191–201, Jun. 2017.

[27] M. Farivar and S. H. Low, "Branch flow model: Relaxations and convexification–Part I," *IEEE Trans. Power Syst.*, vol. 28, no. 3, pp. 2554–2564, Aug. 2013.

[28] Q. Peng, Y. Tang, and S. H. Low, "Feeder reconfiguration in distribution networks based on convex relaxation of OPF," *IEEE Trans. Power Syst.*, vol. 30, no. 4, pp. 1793–1804, Jul. 2015.

[29] Q. Peng and S. H. Low, "Distributed algorithm for optimal power flow on a radial network," in *Proc. IEEE 53rd Conf. Decis. Control*, 2014, pp. 167–172.

[30] Z. Yang, H. Zhong, A. Bose, T. Zheng, Q. Xia, and C. Kang, "A linearized OPF model with reactive power and voltage magnitude: A pathway to improve the MW-only DC OPF," *IEEE Trans. Power Syst.*, vol. 33, no. 2, pp. 1734–1745, Mar. 2018.

[31] *IEEE Standard for Interconnection and Interoperability of Distrib. Energy Resour. With Assoc. Elect. Power Syst. Interfaces*, IEEE Standard 1547-2018 (Revision of IEEE Std 1547-2003), Apr. 2018, pp. 1–138.

[32] Enayati et al, "Impact of IEEE 1547 standard on smart inverters and the applications in power systems," Technical Report PES-TR67.r1, 2020. [Online]. Available: https://www.nrel.gov/grid/ieee-standard-1547/smart-inverters-power-systems.html

[33] "Q at night, reactive power outside feed-in operation with SUNNY CENTRAL 500CP XT - 900CP XT," *SMA Sol. Technol. AG*. [Online]. Available: https://www.sma-america.com/partners/knowledge-base/q-at-night

[34] P. Samadi, H. Mohsenian-Rad, R. Schober, and V. W. S. Wong, "Advanced demand side management for the future smart grid using mechanism design," *IEEE Trans. Smart Grid*, vol. 3, no. 3, pp. 1170–1180, Sep. 2012.

[35] F. Shen, Q. Wu, Y. Xu, F. Li, F. Teng, and G. Strbac, "Hierarchical service restoration scheme for active distribution networks based on ADMM," *Int. J. Elect. Power Energy Syst.*, vol. 118, 2020, Art. no. 105809.

[36] J. Jian, C. Zhang, L. Yang, and K. Meng, "A hierarchical alternating direction method of multipliers for fully distributed unit commitment," *Int. J. Elect. Power Energy Syst.*, vol. 108, pp. 204–217, 2019.

[37] V. Dvorkin, J. Kazempour, L. Baringo, and P. Pinson, "A consensus-ADMM approach for strategic generation investment in electricity markets," in *Proc. IEEE Conf. Decis. Control*, 2018, pp. 780–785.

[38] A. Attarha, P. Scott, and S. Thiébaux, "Affinely adjustable robust ADMM for residential DER coordination in distribution networks," *IEEE Trans. Smart Grid*, vol. 11, no. 2, pp. 1620–1629, Mar. 2020.

[39] F. Qi, M. Shahidehpour, F. Wen, Z. Li, Y. He, and M. Yan, "Decentralized privacy-preserving operation of multi-area integrated electricity and natural gas systems with renewable energy resources," *IEEE Trans. Sustain. Energy*, vol. 11, no. 3, pp. 1785–1796, Jul. 2020.

[40] M. E. Baran and F. F. Wu, "Network reconfiguration in distribution systems for loss reduction and load balancing," *IEEE Trans. Power Del.*, vol. 4, no. 2, pp. 1401–1407, Apr. 1989.

[41] M. L. Bynum et al., *Pyomo–Optimization Modeling in Python*, 3rd ed., vol. 67. Berlin, Germany: Springer, 2021.

[42] M. ApS, "The MOSEK optimization toolbox," 2019. [Online]. Available: http://docs.mosek.com/9.0/toolbox/index.html

[43] F. Borrelli, A. Bemporad, and M. Morari, *Predictive Control for Linear and Hybrid Systems*. Cambridge, U.K.: Cambridge Univ. Press, 2017.

[44] "European network of transmission system operators for electricity," 2022. [Online]. Available: https://transparency.entsoe.eu/dashboard/show

[45] R. D. Zimmerman, C. E. Murillo-Sánchez, and R. J. Thomas, "MATPOWER: Steady-state operations, planning, and analysis tools for power systems research and education," *IEEE Trans. Power Syst.*, vol. 26, no. 1, pp. 12–19, Feb. 2011.

[46] D. T. Feeders, "IEEE PES distribution system analysis subcommittee," 2011. Online Available: http://www.ewh.ieee.org/soc/pes/dsacom/testfeeders/index.html